Solid-State Electronics 229 (2025) 109192

Contents lists available at ScienceDirect

Solid State Electronics

journal homepage: www.elsevier.com/locate/sse

Estimation of the energy levels of the donor–acceptor polymers of organic solar cells using cyclic voltammetry

J.F. Solís-Vivanco [a], Ma.C. Arenas-Arrocena [b], F. DeMoure-Flores [a], A. Velasco-Hernández [a], S.A. Mayén-Hernández [a], J. Cruz-Gómez [c], J. Santos-Cruz [a,*,1]

[a] Facultad de Química, Posgrado en Energía, Universidad Autónoma de Querétaro, Querétaro, México
[b] Research Group of Nanostructures and Biomaterials, Escuela Nacional de Estudios Superiores, Unidad León, UNAM, León 37684 Guanajuato, México
[c] Escuela Superior de Física y Matemáticas del Instituto Politécnico Nacional, Ciudad de México 07738, México

ARTICLE INFO

Keywords:
Cyclic voltammetry
P3HT:$PC_{61}BM$
Energy levels

ABSTRACT

Cyclic voltammetry is a powerful electrochemical tool for obtaining electrical properties as energy levels in polymers. Herein, it has been used to estimate the HOMO and LUMO energy levels of the donor and acceptor polymers, P3HT and $PC_{61}BM$, by varying of GeS_2 nanoparticles, in addition to estimating other parameters such as the E_g, ΔLUMO, and the theoretical V_{oc}. The data obtained were contrasted with an experiment of P3HT:$PC_{61}BM$:GeS_2 inverted organic solar cells to determine the influence of GeS_2 on the energy levels and the reported solar efficiency. Without the addition of nanoparticles to the polymer samples, an E_g of 1.88 eV and 2.25 eV was obtained for P3HT and $PC_{61}BM$, respectively. In addition, a V_{oc} of 1.13 V and an E_{dis} of 0.76 V were found. However, the addition of GeS_2 nanoparticles modified these values, finding a substantial improvement with 0.75 wt% of GeS_2 modifying the E_g to 1.47 eV and 2.52 eV for the P3HT and the $PC_{61}BM$, respectively, with a V_{oc} of 1.31 V and an E_{dis} of 0.15 V. A correlation was found between the estimated theoretical V_{oc} with the experimental V_{oc} and the PCE. Precisely, the best experimental result was with 0.75 wt% of nanoparticles, obtaining a maximum efficiency of 2.18 % and an average device efficiency of 1.99 %.

1. Introduction

Polymeric organic solar cells are being widely investigated due to their optical and electrical properties [1–8]. Some of the most surprising results so far are ternary organic solar cells with efficiencies of 19.1 % or open circuit voltages (V_{oc}) as high as 1.3 V [9–11]. The increase in this type of technology makes it necessary to carry out complementary characterizations of the materials used. Common characterization techniques such as UV–Vis spectroscopy, Raman spectroscopy, scanning electron microscopy, atomic force microscopy, X-ray diffraction, etc. With these characterizations, various parameters such as transmission, absorption, thicknesses, morphology, roughness, and lattice parameters, among others, can be obtained and estimated [12].

Some fundamental parameters for polymeric materials that function as semiconductors are the bandgap (E_g), the energy of the high occupied molecular orbital (HOMO) and the energy of the lowest unoccupied molecular orbital (LUMO) [13–18]. In inorganic semiconductors, E_g is typically estimated by the Tauc method, which relies on the absorption edge observed in the transmission/absorption spectrum of the material and the sample thickness [19,20]. However, organic materials do not exhibit a single absorption edge. Instead, they show a range of absorption, which can make estimating the Eg more challenging and less straightforward.

An advantageous technique to obtain these parameters in organic materials is cyclic voltammetry (CV) [21–23]. CV is an electrochemical technique used to determine the oxidation and reduction processes of molecular species. “CV is also invaluable to study electron transfer-initiated chemical reactions” [24]. In this method, the potential scanning of the working electrode is linearly increased as a function of time, like linear sweep voltammetry. However, once the established potential is reached, the potential of the working electrode increases in the opposite direction until the initial potential is returned to [24,25].

With cyclic voltammetry curves, it is possible to know the potential or the energy the oxidation or reduction of the material. With these data, it is possible to calculate the HOMO, LUMO, and E_g of the materials [26–28]. Furthermore, it is possible to estimate other essential

* Corresponding author.
E-mail address: jsantos@uaq.edu.mx (J. Santos-Cruz).
[1] ORCID: 0000-0002-3619-1713.

https://doi.org/10.1016/j.sse.2025.109192
Received 24 April 2025; Received in revised form 11 June 2025; Accepted 12 July 2025
Available online 13 July 2025

parameters of an active layer in an organic solar cell, such as the theoretical open circuit voltage and the LUMO-LUMO, also called ΔLUMO (which is considered as the energy necessary to dissociate an exciton into a pair electron-hole) [29–33]. These values are critical because they are directly influenced by the energy levels of the materials in the solar device.

On the other hand, there are other techniques to determine these values, such as Ultraviolet photoelectron spectroscopy (UPS), (low-energy) inverse photoemission spectroscopy and photoelectron yield spectroscopy also known as photoelectron spectroscopy in air. Obviously, each of these techniques presents drawbacks during its implementation: While in CV the determination of the position of the redox process peaks can be compromised by the lack of electrochemical or chemical reversibility, in UPS there is a difference in ionization energy between molecules on the surface and in the bulk [34]. However, it has been shown that the variation between the two techniques is minimal, so they could be considered equivalent and reliable enough to use whichever technique and methodology are available, taking into account the principles of resource maximization.

On this research, cyclic voltammetry was performed on samples of P3HT and $PC_{61}BM$ with different percentages of GeS_2 nanoparticles to contrast and complement the electrical results of organic solar cells with this polymeric active layer with the configuration FTO/TiO_2/P3HT:$PC_{61}BM$/MoO_3/Ag. In this way, the results could be correlated with the influence of the energy levels observed through CV.

2. Results and discussions

Fig. 1 shows the cyclic voltammetry curves of P3HT. The solid black lines were performed to obtain the onset reduction potential ($E_{on,\ red}$), meanwhile the dotted blue lines were performed to obtain the onset oxidation potential ($E_{on,\ ox}$). These voltages are located at the intersection or where the extended slope intersects up to a current density equal to zero. The estimated voltages are shown in Table 1.

The $E_{on,\ red}$ in the sample without GeS_2 nanoparticles showed a value of −1.30 V. The value of the consulted references ranges from −1.42 V, remaining relatively close with a difference of 0.12 V [35–37]. When the nanoparticles are added the potential increases (it becomes more positive), going to −0.91 V with 0.25 wt% and finally up to −0.80 V with 0.50 wt%. After this value the $E_{on,\ red}$ decreases to −0.89 V with 0.75 wt % and to −1.23 V with 1.00 wt%. On the other hand, the $E_{on,\ ox}$ in the sample without nanoparticles showed a value of 0.58 V. According to the value of the consulted references ranges from 0.12 V, the difference being wide with 0.46 V. This difference could be due to the manufacturing process and treatment of polymers. When the GeS_2 nanoparticles are added, no trend is observed when varying the percentage of these in the sample. The $E_{on,\ ox}$ is practically the same in the samples with 0.00, 0.50, and 0.75 wt% of GeS_2. However, this value is higher with 0.25 wt% (0.66 V) and lower with 1.00 wt% (0.54 V).

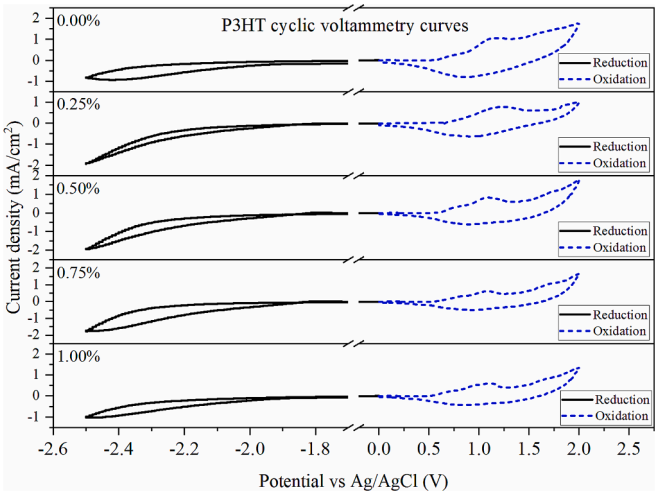

Fig. 1. Cyclic voltammetry curves of P3HT without (0.00 wt%) and with GeS_2 (0.25, 0.50, 0.75, and 1.00 wt%).

Fig. 2 shows the cyclic voltammetry curves of $PC_{61}BM$. As in Fig. 1, the solid black lines represent the experiments to obtain the onset reduction potential ($E_{on,\ red}$), meanwhile the dotted blue lines represent the experiments to obtain the onset oxidation potential ($E_{on,\ ox}$). The $E_{on,\ red}$ of the sample without nanoparticles (0.00 wt%) showed a voltage of −0.55 V, this being higher than the value consulted in the references (−1.11 V) [38–41]. By increasing the percentage of GeS_2 nanoparticles in the $PC_{61}BM$ samples, a similar but inverse trend to that observed with P3HT was observed: The $E_{on,\ red}$ decreased (became more negative) to −0.59 V with 0.25 wt%, to −0.66 V with 0.50 wt% and up to −0.73 V with 0.75 wt%. Finally, this value increased to −0.67 V with 1.00 wt%. Meanwhile, $E_{on,\ ox}$ was found to be quite close: with 0.00 wt% GeS_2 a potential of 1.70 V was estimated; subsequently, it is maintained at approximately 1.80 V with 0.25, 0.50, and 0.75 wt%; finally, with 1.00 wt%, 1.72 V was obtained. Comparing the results obtained with the value consulted in reference (1.76 V), it is possible to see that they are within a similar range. The curves are considered to be relatively well-defined, sufficient for calculating the energy levels. Furthermore, the values found show that $PC_{61}BM$ is a good electron acceptor, while P3HT is considered to have performed well as an electron donor [42].

With the $E_{on,\ red}$ and the $E_{on,\ ox}$ data, it was possible to calculate the E_g of the materials. Graphically, E_g is considered as the interval corresponding to the horizontal section of the CV where the current is equal to zero (in Fig. 1 and Fig. 2). Mathematically, E_g is calculated as the difference between the HOMO and LUMO of the material, but it's proposed calculate by the difference between the $E_{on,\ ox}$ and the $E_{on,\ red}$ (Eq. (1) [35–41]. The results of calculated E_g (for the P3HT and the $PC_{61}BM$) are found in Table 1.

$$E_g = E_{on,ox} - E_{on,red} \tag{1}$$

The E_g of the P3HT presents a clear tendency to decrease, starting at 1.88 eV with 0.00 wt% of GeS_2 nanoparticles and decreasing to 1.57 eV with 0.25 wt% and reaching 1.39 eV 0.50 wt% of GeS_2, after which it increases to 1.47 eV with 0.75 wt% and up to 1.77 eV with 1.00 wt%. In the case of $PC_{61}BM$, the reverse trend was found: it started at 2.25 eV with 0.00 wt% of GeS_2 nanoparticles and increased to 2.39, 2.45 and 2.52 with 0.25, 0.50 and 0.75 wt% of nanoparticles respectively. Finally, the E_g increased to 1.77 eV with 1.00 wt%. It is observed that the polymer donor exhibits an initial narrowing followed by widening of its band gap with increasing GeS_2 nanoparticle content, while $PC_{61}BM$ demonstrates an inverse trend (band gap widening prior to narrowing). This is because GeS_2 is incorporated and generates conductive channels preferentially within the P3HT, allowing the transport of charge carriers, which in turn decreases the energy required for transport, decreasing the $PC_{61}BM$ band gap. Meanwhile, when the $PC_{61}BM$ band gap increases, nanoparticles are incorporated into it, causing an inverse effect. Therefore, a game is observed where the incorporation of GeS_2 simultaneously influences both polymers.

Subsequently, the theoretical open circuit voltage that the polymeric active layer of P3HT: $PC_{61}BM$ would provide was calculated. The theoretical V_{oc} can be calculated as the difference between the LUMO of the acceptor polymer and the HOMO of the donor polymer [43–45]. In the original equation, the V_{oc} is multiplied by "q", which is the elemental charge, and the HOMO-LUMO difference is subtracted by a "Δ", which corresponds to the effective donor/acceptor energy gap (whose value depends on the materials and is found between 0.3 and 0.5) [43]. In this case, by equivalence, the V_{oc} was proposed to be calculated by the difference between the $E_{on,\ ox}$ of the donor polymer and the $E_{on,\ red}$ of the acceptor polymer (Equation (2).

$$V_{oc} = \left|HOMO_{(Donor)} - LUMO_{(Acceptor)}\right| = E_{on,ox(Donor)} - E_{on,red(Acceptor)} \tag{2}$$

Table 1
Electrical properties estimated with the cyclic voltammetry curves for P3HT and $PC_{61}BM$ with GeS_2 (0.0, 0.25, 0.50, 0.75, and 1.00 wt%).

GeS_2	P3HT			$PC_{61}BM$				
	$E_{on,\ red}$	$E_{on,\ ox}$	E_g	$E_{on,\ red}$	$E_{on,\ ox}$	E_g	V_{oc}	E_{dis}
(%)	(V)	(V)	(eV)	(V)	(V)	(eV)	(V)	(V)
Reference	−1.42	0.12	1.54	−1.11	1.76	2.87	1.23	0.31
0.00	−1.30	0.58	1.88	−0.55	1.70	2.25	1.13	0.76
0.25	−0.91	0.66	1.57	−0.59	1.80	2.39	1.26	0.31
0.50	−0.80	0.59	1.39	−0.66	1.79	2.45	1.25	0.14
0.75	−0.89	0.58	1.47	−0.73	1.79	2.52	1.31	0.15
1.00	−1.23	0.54	1.77	−0.67	1.72	2.39	1.21	0.56

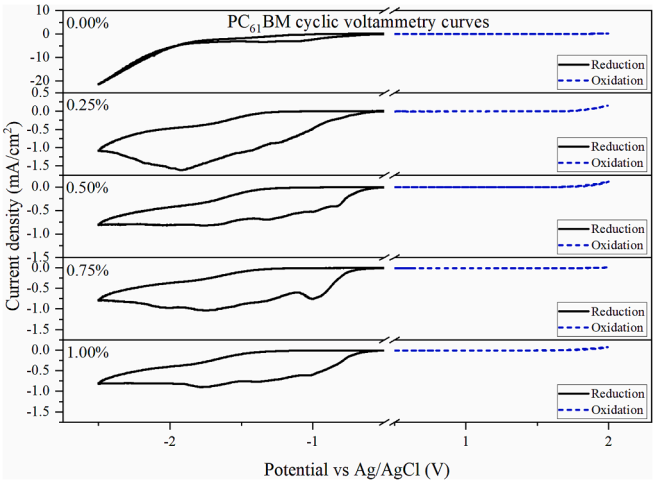

Fig. 2. Cyclic voltammetry curves of $PC_{61}BM$ without (0.00 wt%) and with GeS_2 (0.25, 0.50, 0.75, and 1.00 wt%).

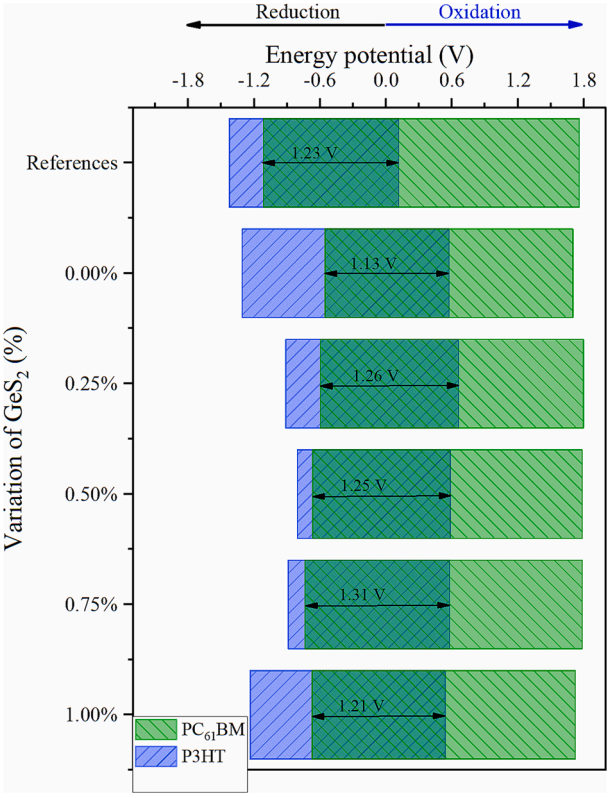

Fig. 3. Energy potential diagram for the active layer P3HT:$PC_{61}BM$ with GeS_2 (0.0, 0.25, 0.50, 0.75, and 1.00 wt%) respectively.

The results are shown in Table 1 and Fig. 3 (dark green section). The V_{oc} of the sample without nanoparticles is 1.13 V, while when they are added this value increases and remains above 1.20 V. With 0.25 and 0.50 wt% the V_{oc} is practically similar with 1.26 and 1.25 V, respectively. The voltage rises to 1.31 V when 0.75 wt% of GeS_2 is added and decreases with 1.00 wt% to 1.21 V. Considering that the increase in V_{oc} benefits the power conversion efficiency (PCE), being directly proportional according to Equation (3) (where J_{sc} is short-circuit current density, FF is fill factor and P_{in} is the input power), it would be evident that the polymeric active layer of P3HT: $PC_{61}BM$ with 0.75 wt% of nanoparticles would present the best PCE concerning the others polymer pairs presented in the experiment [45–48].

$$PCE = \frac{J_{sc} \bullet V_{oc} \bullet FF}{P_{in}} \bullet 100\% \quad (3)$$

In addition, the dissociation energy (E_{dis}) necessary to dissociate the exciton was calculated. This is represented as the difference between the LUMO of the donor polymer ($LUMO_{Donor}$) and the LUMO of the acceptor polymer ($LUMO_{Acceptor}$), also called delta LUMO-LUMO or ΔLUMO [29–33]. Using the CV values obtained, this could be represented as the difference between the $E_{on,\ red}$ of the acceptor polymer and the $E_{on,\ red}$ of the donor polymer and expressed in Equation (4).

$$E_{dis} = LUMO_{(Donor)} - LUMO_{(Acceptor)} = E_{on,\ red(Acceptor)} - E_{on,\ red(Donor)} \quad (4)$$

The calculated E_{dis} are shown in Table 1 and are represented in Fig. 3 as the purple section. The E_{dis} value of the sample without nanoparticles (0.00 wt%) is higher (0.76 V) than the rest of the samples, even than the reference value calculated from the literature. The E_{dis} decreases to 0.31 V with 0.25 wt% of nanoparticles of GeS_2. Subsequently, it decreases to 0.14 and 0.15 V for the samples with 0.50 and 0.75 wt%. Finally, the voltage increases to 0.56 V when 1.00 wt% is added. Some researchers suggest that the optimal and minimum E_{dis} value to separate the electron-hole pair can be between 0.10 and 0.30 V, depending on the materials. The closer the E_{dis} is to the optimal value for the pair of materials, the correct separation of the exciton will be achieved, and the least amount of energy will be lost during the process, making the solar device more efficient.

Fig. 4 and Table 2 show the results of the solar cell experiment with the P3HT:$PC_{61}BM$ polymer layer. The sample without nanoparticles (0.00 wt%) showed the best short circuit current density (J_{sc}) with 12.04 mA/cm^2, but with the lowest experimental V_{oc} of all devices (0.30 V). However, the fill factor (FF) obtained a good result with 0.41, presenting a maximum power conversion efficiency (PCE_{Max}) of 1.49 % and an average power conversion efficiency (PCE_{Av}) of 1.40 %. The J_{sc} tends to decrease the more GeS_2 nanoparticles is added to the active layer. However, the V_{oc} presents an inverse trend as it increases. The FF presents a similar trend as the V_{oc} in the section between 0.25 and 1.00 wt %. Considering that the FF depends largely on the generation and recombination of charge carriers, it could be attributed that a low FF is due to the recombination of charge carriers, while by adding a larger amount of GeS_2 this recombination decreases because the transport of charge carriers through conductive channels is favored. Considering Equation (3), the J_{sc}, the V_{oc}, and the FF are directly proportional to the

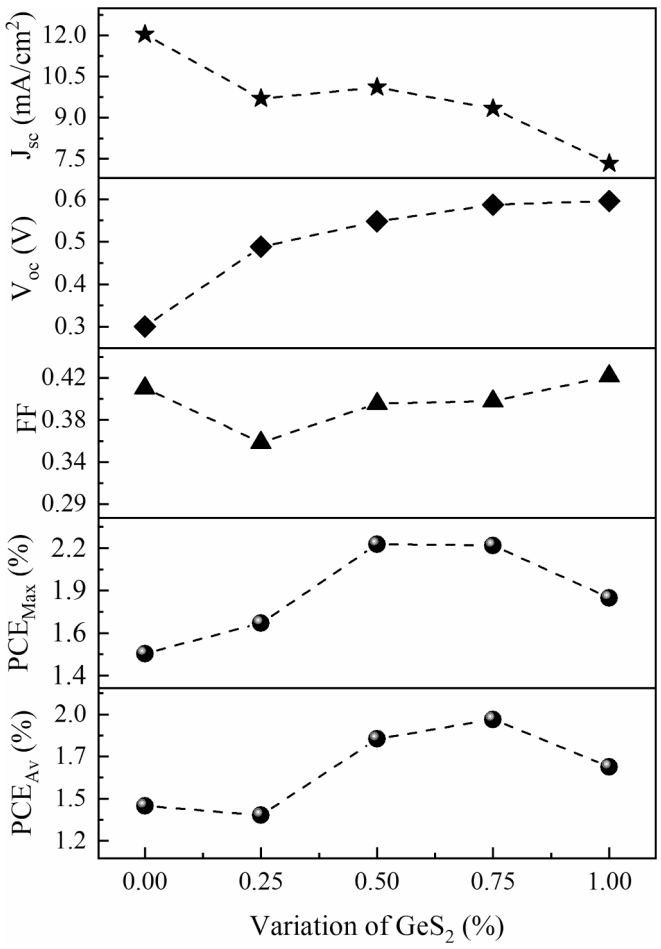

Fig. 4. Electrical properties of the devices structure P3HT:$PC_{61}BM$ doped with GeS_2 (0.0, 0.25, 0.50, 0.75, and 1.00 wt%).

Table 2
Electrical properties of the devices with P3HT:$PC_{61}BM$ without (0.00 wt%) and with GeS_2 (0.25, 0.50, 0.75, and 1.00 wt%).

GeS_2	J_{sc}	V_{oc}	FF	PCE_{Max}	PCE_{Av}
%	mA/cm^2	V		%	%
0.00	12.04	0.30	0.41	1.49	1.40
0.25	9.70	0.49	0.36	1.68	1.34
0.50	10.11	0.55	0.39	2.18	1.86
0.75	9.33	0.59	0.40	2.18	1.99
1.00	7.33	0.60	0.42	1.84	1.67

PCE. Because two of the three variables increase depending on the increase in nanoparticles in the active layer, the PCE increases to its maximum at 0.75 wt% with a PCE_{Max} of 2.18 % and a PCE_{Av} of 1.99 %. However, both the maximum efficiency and the average efficiency decrease to 1.00 wt%. This is attributed to the fact that, according to the estimated results in Table 1, the theoretical V_{oc} decreases and the E_{dis} increases, affecting the PCE at this point.

The PCE_{Max} increases from 1.49 % without nanoparticles to 1.68 % with 0.25 wt% and then to 2.18 wt% with 0.50 wt% and remaining at 0.75 wt%. This would be mainly influenced by the E_{dis} estimated and presented in Table 1, where it was maintained between 0.14 and 0.15 V for 0.50 and 0.75 wt% GeS_2. Finally, the PCE_{Max} decreases to 1.84 % with 1.00 wt%. On the other hand, the PCE_{Av} is found at 1.40 % for the device without nanoparticles, subsequently decreasing to 1.34 % with 0.25 wt% of GeS_2. Then it increases to 1.86 % and 1.99 % with 0.50 and 0.75 wt%, finally decreasing again to 1.67 % with 1.00 wt%. In this, the estimated theoretical V_{oc} could play an important role, which tends to increase with the addition of GeS_2 nanoparticles. The theoretical V_{oc} estimated in Table 1 and the one obtained experimentally in Table 2 have a similar trend, but they break with 1.00 wt%. Despite this, a good correlation is considered between the theoretically estimated data and the experimental ones. The observed variations could be due to natural variations between samples. The results are similar to those found in previous works, with the difference that a double electron transport layer (DETL) was previously used [49]. According to the literature, where nanoparticles or interlayers have been added, in this case, GeS_2 in the active layer matrix can promote improved charge collection and suppress carrier recombination losses. Furthermore, it can provide hole transport channels, effectively enhancing the transport of holes generated by self-dissociation, resulting in improved FF [50–53]. Furthermore, as a second cause of the low FF, it is concluded that there is the presence of hole traps or energy traps, either inside or on the surface of the material, especially near the metallic contacts. Although, initially, the addition of sulfide decreases the FF due to the minimal distribution of the nanoparticles and the close proximity between them, when a larger amount is added, the FF is recovered due to the decrease in the presence of traps [42]. This effect is most evident in the V_{oc}, which increases from 0.3 V to 0.6 V. However, the difference between the theoretical V_{oc} and the experimental V_{oc} is initially due to the fact that the theoretical part is based on an idealized model and is a direct consequence of the material properties, while an experimental development involves real limitations, such as material imperfections, surface effects, and device manufacturing limitations [54–56]. On the other hand, the effect can be expressed with the quantum density of states model, where the set of probabilities in which the V_{oc} of the material can be found is determined by the number of quantum states available per unit of energy and volume, being exactly 0.6 V in the case of P3HT:$PC_{61}BM$ [7,32]. Also, this experiment would mainly reinforce that it is possible to modify the energy levels of the active layer and increase the energy conversion efficiency. In addition, it would serve as complementary evidence to explain the increase in efficiency.

3. Conclusions

Capacitance vs voltage characterization demonstrated being a powerful tool to obtain electrical parameters for polymeric materials. Using the $E_{on,\ red}$ and $E_{on,\ ox}$ it was possible to estimate the bandgap, the theoretical open circuit voltage, and the exciton dissociation energy. In addition, by comparing the samples without nanoparticles with the samples with GeS_2 it was possible to demonstrate that these nanoparticles play a fundamental role in modifying the energy levels. While the sample without nanoparticles showed a theoretical V_{oc} of 1.13 V, with 0.75 wt% of GeS_2 it reached 1.31 V. On the other hand, with the same percentage of nano-particles the E_{dis} was estimated at 0.15 V, and without nanoparticles it reached 0.76 V. Although the minimum E_{dis} achieved was 0.14 V with 0.50 wt%, the sample with 0.75 wt% showed better results for both V_{oc} and E_{dis}. When contrasted with the efficiencies, the expected results were observed and coherent in terms of PCE, since it was expected that the best solar device was the one with 0.75 wt% of GeS_2, obtaining a J_{sc} of 9.33 mA/cm^2, a V_{oc} of 0.59 V, a FF of 0.40, a PCE_{Max} of 2.18 %, and PCE_{Av} of 1.99 %.

4. Materials and methods

FTO covered glass substrates were cut (~1 cm × 1.5 cm) and cleaned in ultrasonic bath sequentially for 15 min in a detergent solution, acetone, and ethanol each. In a nitrogen atmosphere glove box, nanoparticles of GeS_2 were dissolved onto o-dichlorobenzene and added P3HT and $PC_{61}BM$ to obtain solutions of P3HT and $PC_{61}BM$ in the proportion of 12.5 mg/mL with 0.00, 0.25, 0.50, 0.75, and 1.00 wt% of GeS_2. The same solution, varying the percentages of sulfur, was used for the construction of all the devices. These solutions were spin-coated over

FTO substrates at 500 RPM for 1 min. After that, layers were annealed at 120 °C for 10 min over a hotplate.

A 0.1 M tetrabutylammonium hexafluorophosphate (Bu_4NPF_6) in acetonitrile solution was made and employed as electrolyte. Each sample was placed in the working electrode of an EuroCell electrochemical cell kit. Also, a platinum bar was used as a counter electrode and a Ag/AgCl solution as reference electrode. All measurements were performed using a Gamry Interface 1000 potentiostat/galvanostat/ZRA device and enough solution was prepared to perform the entire experiment. The same amount of solution was measured for each measurement. The area of each sample was ensured to be homogeneous and consistent across all samples. The effective areas were calculated and used during the measurement. The set of connections on the electrodes and on the sample were always placed in tge same position to reduce possible variations.

For solar cell devices after the FTO cleaning a layer of TiO_2 was spin-coated at 1500 RPM for 1 min and annealed at 550 °C for 1 h. Subsequently, the active layer was spin-coated at 500 RPM for 1 min from P3HT:$PC_{61}BM$ solutions in the proportion of 25 mg/mL with 0.00, 0.25, 0.50, 0.75, and 1.00 wt% of GeS_2. Then, a MoO_3 layer and a Ag contact was deposited by PVD system using a shadow mask to obtain thicknesses of ~ 10 and ~ 100 nm, respectively. It should be noted that these layers were deposited at the same time on all devices to ensure uniform thickness across all of them. A total of 12 cells were used for each sulfide percentage variation. Current density-voltage data were obtained from the solar simulator model LCS-100 calibrated with AM 1.5.

CRediT authorship contribution statement

J.F. Solís-Vivanco: Writing – original draft, Methodology, Investigation. **Ma.C. Arenas-Arrocena:** Writing – review & editing, Validation, Methodology, Data curation. **F. DeMoure-Flores:** Writing – review & editing, Validation, Methodology, Conceptualization. **A.Velasco-Hernández:** Writing – original draft, Validation, Methodology, Investigation. **S.A. Mayén-Hernández:** Writing – review & editing, Validation, Formal analysis, Conceptualization. **J. Cruz-Gómez:** Writing – original draft, Methodology. **J. Santos-Cruz:** Supervision, Project administration, Funding acquisition, Formal analysis, Conceptualization.

Funding

Authors acknowledge to CONAHCYT, for doctoral degree scholarship to JFSV.

Declaration of competing interest

The authors declare that they have no known competing financial interests or personal relationships that could have appeared to influence the work reported in this paper.

Acknowledgments

Authors acknowledge to CONAHCYT, for doctoral degree scholarship to JFSV and for the partial financial support and the project FQST 2021.

Data availability

The data that support the findings of this study are not openly available and are available from the corresponding author upon reasonable request. The data is in the Advanced Materials Laboratory of the Autonomous University of Queretaro.

References

[1] Pathak D, Wagner T, Adhikari T, Nunzi JM. AgInSe2.PCBM.P3HT inorganic organic blends for hybrid bulk heterojunction photovoltaics. Synth Met 2015;200:102–8. https://doi.org/10.1016/j.synthmet.2015.01.001.
[2] Holliday S, et al. High-efficiency and air-stable P3HT-based polymer solar cells with a new non-fullerene acceptor. Nat Commun 2016;7:1–11. https://doi.org/10.1038/ncomms11585.
[3] Aruna P, Joseph CM. Annealing effects on the electrical properties of spin coated poly (3-hexylthiophene) (P3HT) thin films. Mater Sci Semicond Process 2017;61:39–44. https://doi.org/10.1016/j.mssp.2016.12.041.
[4] Hösel M, Angmo D, Krebs F. Organic solar cells (OSCs). In: Handbook of Organic Materials for Optical and (Opto)Electronic Devices: Properties and Applications; 2013. p. 473–507.
[5] Trung M, et al. Solar energy materials & solar cells polymeric solar cells based on P3HT: PCBM: role of the casting solvent. Sol Energy Mater Sol Cells 2011;95(12):3408–18. https://doi.org/10.1016/j.solmat.2011.07.039.
[6] Wu Q, Bhattacharya M, Moore LMJ, Morgan SE. Air processed P3HT: PCBM photovoltaic cells: morphology correlation to annealing. Degrad Recovery 2014:1–10. https://doi.org/10.1002/polb.23605.
[7] Amador Bedolla C, Olivares Amaya R, Hachmann J, Aspuru Guzik A. Organic photovoltaics. In: Rajan K, editor. Informatics for Materials Science and Engineering. Elsevier; 2013. p. 423–42.
[8] A. Supriyanto, A. Supriyanto, A. Mustaqim, D. Qin, W. Wang, M. Wang, Optical and Morphological Properties of P3HT and P3HT: PCBM Thin Films Used in Photovoltaic Applications Optical and Morphological Properties of P3HT and P3HT: PCBM Thin Films Used in Photovoltaic Applications, pp. 0–6, doi: 10.1088/1757-899X/374/1/012015.
[9] Dai T, et al. Modulation of molecular quadrupole moments by phenyl side-chain fluorination for high-voltage and high-performance organic solar cells. J Am Chem Soc 2025;147(5):4631–42. https://doi.org/10.1021/jacs.4c17140.
[10] Wang Z, et al. Dithienoquinoxalineimide-based polymer donor enables all-polymer solar cells over 19 \% efficiency. Angew Chemie Int Ed 2024;63(21):e202319755. https://doi.org/10.1002/anie.202319755.
[11] Li X, et al. Benzotriazole-based 3D four-arm small molecules enable 19.1 % efficiency for PM6: Y6-based ternary organic solar cells. Angew Chem Int Ed Engl 2023;62(39). https://doi.org/10.1002/anie.202306847.
[12] Saleh TA. Chapter 7 - Characterization and description of adsorbents and nanomaterials. In: Saleh T, editor. Surface Science of Adsorbents and Nanoadsorbents, vol. 34. Elsevier; 2022. p. 199–232.
[13] Derouiche H, Djara V. Impact of the energy difference in LUMO and HOMO of the bulk heterojunctions components on the efficiency of organic solar cells. Sol Energy Mater Sol Cells 2007;91(13):1163–7. https://doi.org/10.1016/j.solmat.2007.03.015.
[14] Rwenyagila E. A review of organic photovoltaic energy source and its technological designs. Int J Photoenergy Oct. 2017;2017:1–12. https://doi.org/10.1155/2017/1656512.
[15] Hagberg DP, et al. Tuning the HOMO and LUMO energy levels of organic chromophores for dye sensitized solar cells. J Org Chem Dec. 2007;72(25):9550–6. https://doi.org/10.1021/jo701592x.
[16] Scharber M, Sariciftci N. Low Band Gap Conjugated Semiconducting Polymers. Adv. Mater. Technol. 2021;6:2000857. https://doi.org/10.1002/admt.202000857.
[17] Wang Y, et al. Bandgap engineering of organic semiconductors for highly efficient photocatalytic water splitting. Adv Energy Mater 2018;8(24):1801084. https://doi.org/10.1002/aenm.201801084.
[18] Costa JCS, Taveira RJS, Lima CFRAC, Mendes A, Santos LMNBF. Optical band gaps of organic semiconductor materials. Opt Mater (Amst) 2016;58:51–60. https://doi.org/10.1016/j.optmat.2016.03.041.
[19] Makuła P, Pacia M, Macyk W. How to correctly determine the band gap energy of modified semiconductor photocatalysts based on UV–Vis spectra. J Phys Chem Lett 2018;9(23):6814–7. https://doi.org/10.1021/acs.jpclett.8b02892.
[20] Solís-Vivanco JF, Aruna-Devi R, Arenas-Arrocena MC, Sosa-Domínzuez A, De Moure-Flores FJ, Santos-Cruz J. Double ETL in ITO-free poly-3-hexylthiophene-based organic solar cells. In: 2021 18th International Conference on Electrical Engineering, Computing Science and Automatic Control (CCE); 2021. p. 1–5. https://doi.org/10.1109/CCE53527.2021.9633072.
[21] L. N. Leonat, G. B. Sbarcea, and I. V. Branzoi, Cyclic voltammetry for energy levels estimation of organic materials, 2013, [Online]. Available: https://api.semanticscholar.org/CorpusID:27714384.
[22] Forster R, Cumba L. Cyclic Voltammetry of Organic Compounds 2018.
[23] Kissling GP, Ruhstaller B, Pernstich KP. Measuring frontier orbital energy levels of OLED materials using cyclic voltammetry in solution. Org. Electron. 2023;122:106888. https://doi.org/10.1016/j.orgel.2023.106888.
[24] Elgrishi N, Rountree KJ, McCarthy BD, Rountree ES, Eisenhart TT, Dempsey JL. A Practical beginner's guide to cyclic voltammetry. J. Chem. Educ. 2018;95(2):197–206. https://doi.org/10.1021/acs.jchemed.7b00361.
[25] Francis S, Koshy EP, Mathew B. Chapter 7 - Electroanalytical techniques: a tool for nanomaterial characterization. In: Thomas S, Kalarikkal N, Abraham ARBT-D, editors. Micro and Nano Technologies, Fabrication, and Characterization of Multifunctional Nanomaterials. Elsevier; 2022. p. 163–75.
[26] Adeniyi AA, Ngake TL, Conradie J. Cyclic voltammetric study of 2-Hydroxybenzophenone (HBP) derivatives and the correspondent change in the orbital energy levels in different solvents. Electroanalysis 2020;32(12):2659–68. https://doi.org/10.1002/elan.202060163.
[27] Sworakowski J. How accurate are energies of HOMO and LUMO levels in small-molecule organic semiconductors determined from cyclic voltammetry or optical

spectroscopy? Synth. Met. 2018;235:125–30. https://doi.org/10.1016/j.synthmet.2017.11.013.
[28] Shafiee A, Mat Salleh M, Yahaya M. Determination of HOMO and LUMO of [6,6]-Phenyl C61-butyric Acid 3-ethylthiophene Ester and Poly (3-octyl-thiophene-2, 5-diyl) through Voltametry Characterization. Sains Malaysiana 2011;40:173–6.
[29] Zhu Y, Zhao F, Wang W, Li Y, Zhang S, Lin Y. Exciton binding energy of non-fullerene electron acceptors. Adv Energy Sustain Res 2022;3(4):2100184. https://doi.org/10.1002/aesr.202100184.
[30] Ono S, Ohno K. Origin of Charge Transfer Exciton Dissociation in Organic Solar Cells. Rijeka: IntechOpen; 2017.
[31] Clarke T. How to split an exciton. Nat. Energy 2020;5. https://doi.org/10.1038/s41560-020-00689-2.
[32] Sánchez F, Amador-Bedolla C, Sánchez V, Wang C. Exciton dissociation in correlated molecular photocells. J. Phys. Chem. Solids 2021;152:109966. https://doi.org/10.1016/j.jpcs.2021.109966.
[33] Emelianova EV, van der Auweraer M, Bässler H. Hopping approach towards exciton dissociation in conjugated polymers. J. Chem. Phys. 2008;128(22):224709. https://doi.org/10.1063/1.2938088.
[34] Willems R, Weijtens C, Vries X, Coehoorn R, Janssen R. Relating frontier orbital energies from voltammetry and photoelectron spectroscopy to the open-circuit voltage of organic solar cells. Adv Energy Mater 2019;9:1803677. https://doi.org/10.1002/aenm.201803677.
[35] Acevedo-Peña P, Baray-Calderón A, Hu H, González I, Ugalde-Saldivar VM. Measurements of HOMO-LUMO levels of poly(3-hexylthiophene) thin films by a simple electrochemical method. J Solid State Electrochem 2017;21(8):2407–14. https://doi.org/10.1007/s10008-017-3587-2.
[36] S. d s,, et al. Low cost synthesis and characterization of donor P3HT polymer for fabrication of organic solar cell. IOP Conf Ser Mater Sci Eng 2022;1221(1):12060. https://doi.org/10.1088/1757-899X/1221/1/012060.
[37] Choi WT, Bard AJ. Doping of the semiconducting polymer poly(3-hexylthiophene) (P3HT) in organic photoelectrochemical cells. J Phys Chem C 2020;124(6):3439–47. https://doi.org/10.1021/acs.jpcc.9b09735.
[38] K. Kutlu et al., Energy-band diagram of PCDTBT, PCBM and blend by cyclic voltammetry and UV-visible measurements, vol. 1569. 2013.
[39] Thawarkar S, et al. Trifluoromethyl-directed supramolecular self-assembly of fullerenes: synthesis characterization and photovoltaic applications. ChemistrySelect 2020;5:1115–21. https://doi.org/10.1002/slct.201902974.
[40] Labrunie A, et al. CuAAC-based assembly and characterization of a new molecular dyad for single material organic solar cell. Metals (Basel) 2019;9:618. https://doi.org/10.3390/met9060618.
[41] Yoo S, Kum JM, Cho SO. Tuning the electronic band structure of PCBM by electron irradiation. Nanoscale Res Lett 2011;6:545. https://doi.org/10.1186/1556-276X-6-545.
[42] Duan C, et al. Toward green solvent processable photovoltaic materials for polymer solar cells: the role of highly polar pendant groups in charge carrier transport and photovoltaic behavior. Energy Environ Sci 2013;6(10):3022–34. https://doi.org/10.1039/C3EE41838C.
[43] Lee M-H. Identifying correlation between the open-circuit voltage and the frontier orbital energies of non-fullerene organic solar cells based on interpretable machine-learning approaches. Sol. Energy 2022;234:360–7. https://doi.org/10.1016/j.solener.2022.02.010.
[44] Bouzzine SM. Theoretical investigation on the optoelectronic properties of non-centrosymmetric D-A-D hexaazatriphenylene derivatives for photovoltaic applications. Mediterr J Chem 2015;4:168–75. https://doi.org/10.13171/mjc44/015020713/bouachrine.
[45] Aziz EA, Amine A, Hamidi M, Bouachrine M. Conjugated molecules consisting of thienylenevinylene-co-cyanophenylene as donor materials for bulk heterojunction solar cells. J Mater Environ Sci 2018;9:918–27. https://doi.org/10.26872/jmes.2018.9.3.102.
[46] Hu Z, et al. A critical review on semitransparent organic solar cells. Nano Energy 2020;78:105376. https://doi.org/10.1016/j.nanoen.2020.105376.
[47] Gavrik A, et al. Spectral technique for accurate efficiency measurements of emerging solar cells. Sol. Energy 2020;206:770–7. https://doi.org/10.1016/j.solener.2020.06.015.
[48] M. Hosseinzadeh Dizaj, Calculating the efficiency of perovskite solar cells using formula (PCE= [(Voc.Jsc. FF)/Pin].100%) and increasing and obtaining the quality of the HTL layer in perovskite solar cells using formula (FF=Pmax/ (Voc.Jsc)), vol. 1, 2024.
[49] Solís-Vivanco JF, De Moure-Flores F, Arenas-Arrocena MC, Santos-Cruz J. Effect in the power conversion efficiency in inverted P3HT organic solar cells doped with nano-germanium sulfide. J. Mater. Res. 2023;38(9):2413–21. https://doi.org/10.1557/s43578-023-00971-5.
[50] Tian H, et al. Over 19.2% efficiency of layer-by-layer organic photovoltaics by ameliorating exciton dissociation and charge transport. Adv Funct Mater 2025;35. https://doi.org/10.1002/adfm.202422867.
[51] Tian H, et al. Over 19.2% efficiency of layer-by-layer organic photovoltaics enabled by a highly crystalline material as an energy donor and nucleating agent. Energy Environ Sci 2024;17(14):5173–82. https://doi.org/10.1039/D4EE01717J.
[52] Zhou H, et al. Over 18.2% efficiency of layer–by–layer all–polymer solar cells enabled by homoleptic iridium(III) carbene complex as solid additive. Sci Bull 2024;69(18):2862–9. https://doi.org/10.1016/j.scib.2024.07.027.
[53] Ni Y, et al. Achieving 18.29% efficiency of layer-by-layer all polymer solar cells enabled by iridium complex as energy donor and crystallizing agent. Chem Eng J 2025;507:160359. https://doi.org/10.1016/j.cej.2025.160359.
[54] Orlowski BA, et al. Extended defect States in CdTe/ZnTe Photojunction. Acta Phys. Pol. A 2022;141:548–53. https://doi.org/10.12693/APhysPolA.141.548.
[55] Hernández-Ortiz OJ, et al. Theoretical-experimental correlation of Voc in isoindigo-based small molecules for photovoltaic applications. Chem Phys Impact 2025;10:100808. https://doi.org/10.1016/j.chphi.2024.100808.
[56] Zhou X, Song C, Liu J. Impact of temperature and microstructure on the emission characteristics of VOC in porous building materials. Proc Eng 2015;121:1067–75. https://doi.org/10.1016/j.proeng.2015.09.104.